Alteration of Membrane Compositional Asymmetry by $LiCoO_2$ Nanosheets

Merve Doğangün,[†] Mimi N. Hang,[‡] Julianne M. Troiano,[†] Alicia C. McGeachy,[†] Eric S. Melby,[§] Joel A. Pedersen,[‡,§] Robert J. Hamers,[‡] and Franz M. Geiger*[,†]

[†]Department of Chemistry, Northwestern University, Evanston, Illinois 60208, United States and [‡]Department of Chemistry and [§]Environmental Chemistry and Technology Program, University of Wisconsin, Madison, Wisconsin 53706, United States

ABSTRACT Given the projected massive presence of redox-active nanomaterials in the next generation of consumer electronics and electric vehicle batteries, they are likely to eventually come in contact with cell membranes, with biological consequences that are currently not known. Here, we present nonlinear optical studies showing that lithium nickel manganese cobalt oxide nanosheets carrying a negative ζ-potential have no discernible consequences for lipid alignment and interleaflet composition in supported lipid bilayers formed from zwitterionic and negatively charged lipids. In contrast, lithiated and delithiated $LiCoO_2$ nanosheets having positive and neutral ζ-potentials, respectively, alter the compositional asymmetry of the two membrane leaflets, and bilayer asymmetry remains disturbed even after rinsing. The insight that some cobalt oxide nanoformulations induce alterations to the compositional asymmetry in idealized model membranes may represent an important step toward assessing the biological consequences of their predicted widespread use.

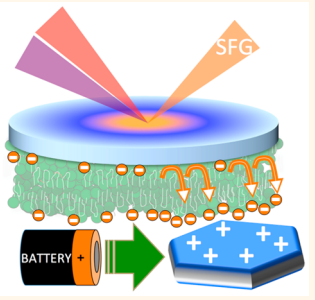

KEYWORDS: phospholipid bilayer asymmetry · nano–bio interface · sum-frequency generation · secondary ion mass spectrometry · transbilayer movement · silica/water interfaces

In portable electronics, $LiCoO_2$ is among the most commonly used commercial cathode materials.[1−3] Nano- and microformulated $LiCoO_2$, in particular, features high capacity and cyclability,[4,5] while a related material, lithium nickel manganese cobalt oxide (NMC), offers improved rate performance at a reduced cost.[6−8] $LiCoO_2$ and NMC nanoformulations are projected to be widely used in consumer electronics, all-electric/hybrid vehicle batteries, and in grid energy storage applications.[9−12] The redox potentials of these materials overlap with those of several biologically important redox pairs, suggesting that exposure to them may perturb cellular function.[13,14] The formulations of these nanoscale materials need to be developed while keeping the possibility in mind that these materials may enter the environment, where they may come in contact with unicellular and multicellular organisms. Given the unknown biological consequences of such interactions, we believe that it is critical to develop a molecular level understanding of how these nanomaterials interact with biological interfaces, including lipid membranes.[15−17] Our work makes a first step in this direction by using a molecular approach to probe the interaction of $LiCoO_2$ and NMC nanosheets with supported phospholipid bilayers. We find that some cobalt oxide nanoformulations cause alterations to the compositional asymmetry in our idealized model membranes that persist even upon rinsing, and that some of the nanosheets irreversibly interact with the membranes under the conditions of our experiments. This finding is important as alterations in the compositional asymmetry of membranes are known to signal multiple negative consequences for cellular processes, as discussed recently.[18−20]

Our choice to focus on lipid bilayer systems is motivated by recent explorations of the uptake and accumulation of various engineered nanomaterials, typically composed of redox-inactive cores, by prokaryotic and eukaryotic cells, as well as their interaction with model cell membranes.[21−24] In particular, nanoparticle–phospholipid bilayer interactions have been investigated through a host of analytical techniques, including fluorescence spectroscopy, electrochemical impedance spectroscopy, quartz crystal microbalance with dissipation monitoring (QCM-D), and scanning probes.[25−30] However, these methods require tagged or labeled molecules, lack inherent surface

* Address correspondence to geigerf@chem.northwestern.edu.

Received for review March 6, 2015 and accepted August 6, 2015.

Published online August 06, 2015
10.1021/acsnano.5b01440

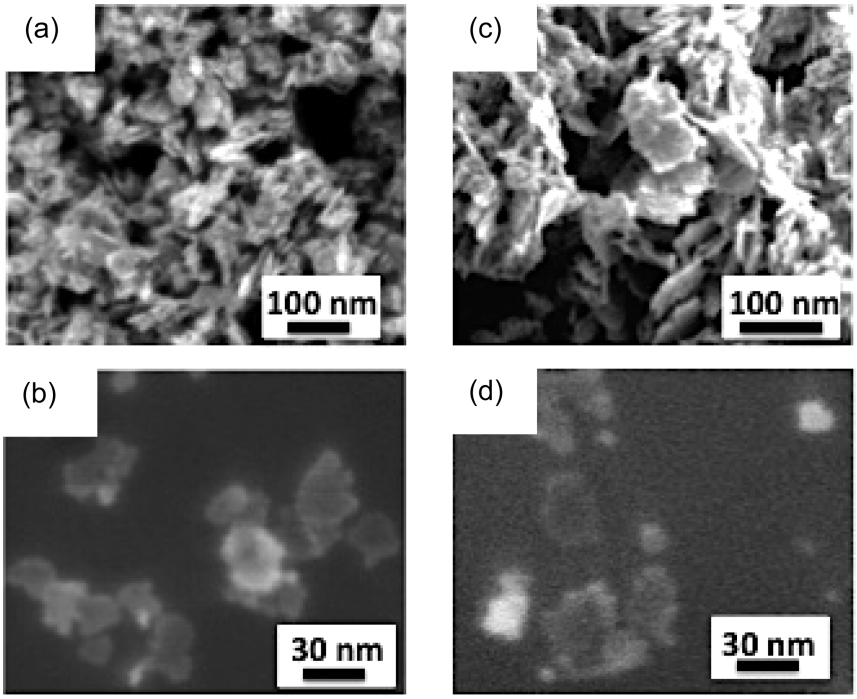

Figure 1. Scanning electron microscopy shows that the (a,b) sheet-like structure of $LiCoO_2$ is retained (c,d) after electrochemical delithiation. (a,c) Clumps of the nanosheets and (b,d) individually resolved nanosheets.

sensitivity, or are not chemically specific. In contrast to these methods, vibrational sum-frequency generation (SFG) spectroscopy is applicable to study the various oscillators and determine structural and orientational information about them, directly at aqueous/solid interfaces with surface specificity.[31−33] SFG has been shown to provide structural and orientational information on supported lipid bilayer (SLB) interfaces in aqueous environments.[32,34−36] SFG has also been used to probe phase transitions of lipid bilayers,[37,38] kinetics of transbilayer movement of lipids,[39−46] bilayer asymmetry,[18] and protein−lipid interactions.[44,47−49] The technique is particularly powerful when applied in conjunction with complementary methods when probing nanoparticle−membrane interactions, as we recently showed for gold metal nanoparticle−membrane interactions.[50]

The present work aims to address the molecular basis of the interactions of lithiated and delithiated $LiCoO_2$ nanosheets, as well as those composed of NMC, with single and binary component supported phospholipid bilayers under environmentally relevant pH and ionic strength conditions. (SEM images of synthesized $LiCoO_2$ and delithiated $LiCoO_2$ nanosheets are shown in Figure 1.) We present results from SFG spectroscopy experiments that probe changes in the structure and chemical composition of supported lipid bilayers held at constant temperature, ionic strength, and pH. Our studies provide evidence that compositional asymmetry is induced between the two leaflets of binary phospholipid mixtures near the gel-to-liquid crystalline phase transition temperature (T_m), upon addition of positively charged lithiated and near neutral delithiated $LiCoO_2$ nanosheets under isothermal conditions. 1,2-Dimyristoyl-*sn*-glycero-3-phosphocholine (DMPC) was selected as a model lipid since zwitterionic phosphocholine-derived lipids are among the most common phospholipids found in eukaryotic membranes.[51] 1,2-Dimyristoyl-*sn*-glycero-3-phospho-(1-*rac*-glycerol) (DMPG) was chosen because its T_m is comparable with that of DMPC and because the negatively charged headgroup allows investigations into the importance of electrostatics in the interaction. 1,2-Ditetradecanoyl-*sn*-glycero-3-phospho-L-serine (DMPS) was selected as a second anionic phospholipid because phosphatidylserine is among the most abundant anionic headgroups in eukaryotic cell membranes.[52] Given recent work by Stanglmaier *et al.*[19] and by Rossetti *et al.*,[20] and given that we use fused silica as a support for the lipid bilayers, it is likely that some degree of compositional asymmetry is present within the bilayers prior to particle exposure under the conditions of our experiments.

RESULTS AND DISCUSSION

Particle Attachment. SHG and QCM-D measurements showed no attachment of lithiated $LiCoO_2$ particles to the supported lipid bilayers (see Supporting Information Figures S1 and S2). While the SHG limit of detection for the particles under investigation here is not known, the QCM-D limit of detection is on the order of 1 ng/cm^2. We therefore proceeded to probe for the Li^+ ions of the $LiCoO_2$ nanosheets by using time-of-flight secondary ion mass spectrometry (ToF-SIMS). Figure 2 shows the ToF-SIMS spectra of 9:1 DMPC/DMPG

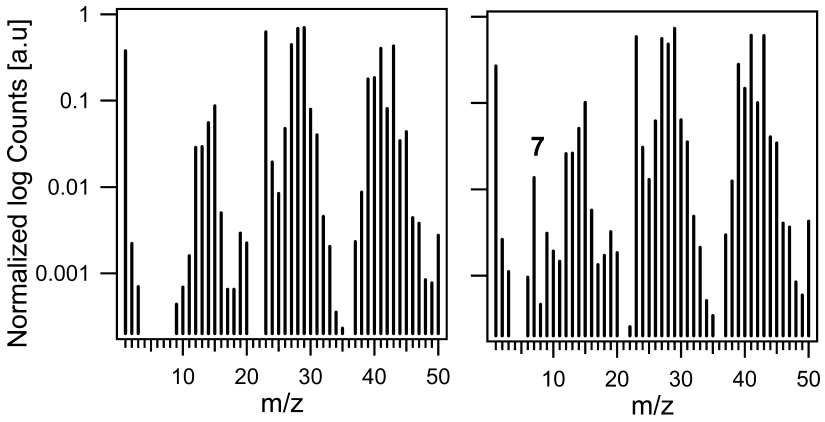

Figure 2. Averaged ToF-SIMS spectra of bilayers formed from 9:1 mixture of DMPC/DMPG in 0.01 M Tris buffer, 0.1 M NaCl, at 23 °C and pH 7.4 (*m/z* 0−50) (left) before the addition of nanosheets and (right) upon exposure to $LiCoO_2$ nanosheets and rinsing with 0.01 M Tris buffer solution in the presence of 0.1 M NaCl at 23 °C and pH 7.4. Additional spectra out to 200 amu shown in the Supporting Information as averages of triplicate measurements of three bilayer samples before and after exposure to $LiCoO_2$ nanosheets (Figure S4).

bilayers before and after interaction with 5 mg/L of $LiCoO_2$ particle solution over the spectral region of interest (*m/z* 0−50). Following particle exposure and rinse, the spectrum shows the presence of a mass peak at *m/z* = 7 corresponding to the atomic mass of lithium. Control experiments carried out with 1 mg/L of LiCl solution showed no lithium present in the bilayer spectrum (Figure S3). ToF-SIMS has been previously applied in structural analysis of lipid monolayers and bilayers.[53,54] ToF-SIMS spectra of the bilayers made of a 9:1 mixture of DMPC/DMPG lipids before and after exposure to $LiCoO_2$ nanosheets in the *m/z* range of 0−200 are given in Figure S4.

We also employed SEM/EDS to provide further evidence of particles on the bilayer after rinsing. Figure 3 shows the SEM image and the corresponding EDS spectra on different spots of an ultraflat SiO_2 wafer with a bilayer prepared from a 9:1 mixture of DMPC/DMPG lipids. Following nanosheet exposure and rinse, localized regions of the bilayer contained $LiCoO_2$ nanosheets which were observed by SEM/EDS. Figure 3 shows that $LiCoO_2$ nanosheets have distinct flake-like structures, which can be easily distinguished from larger cubic structures of NaCl. EDS spectrum 1 in Figure 3 shows that the cubic structures exhibit Na (1.04 keV) and Cl (2.62 keV) signals in EDS, further confirming our ability to distinguish the difference between nanosheets and salt. EDS spectrum 2 shows that in a region void of nanosheets or salt features, only Si (1.84 keV) and O (0.52 keV) signals originating from the underlying SiO_2 substrate are detected. EDS spectrum 3 shows that the region of $LiCoO_2$ nanosheets exhibits Co signals (0.79 and 7.65 keV). The identity of the peak at 3.4−3.5 keV that is evident in the EDS spectra is not known. It is too far from Ca (3.69 keV) and K (3.312) to be either of those elements. Together with ToF-SIMS data presented in Figure 2, the SEM/EDS data clearly show that our rinsing procedures do not quantitatively remove the $LiCoO_2$ nanosheets.

$LiCoO_2$ Particles Elicit Increases in SFG Signal Intensity from 9:1 DMPC/DMPG Bilayers. Having shown that $LiCoO_2$ particles are likely to be present at the membrane surface, we applied SFG spectroscopy to study their impact on molecular order along the lipid carbon chains by using our recently described approach.[50] Specifically, we applied SFG to probe the structural changes among the methyl groups of the alkyl tails upon interaction with 5 mg/L of $LiCoO_2$. A representative SFG spectrum of a 9:1 DMPC/DMPG bilayer in 0.01 M Tris buffer in the presence of 0.1 M NaCl at pH 7.4 is shown in Figure 4a. As we reported earlier,[50] we typically observe three vibrational features centered at 2875, 2907, and 2950 cm^{-1} remain invariant with ionic strength between 0.001 and 0.1 M NaCl concentration. To probe the structural changes of the bilayer, we monitor the 2875 cm^{-1} peak (Figure 4), which can be attributed to the CH_3 symmetric stretch of the alkyl tails, as suggested by Liu and co-workers.[18,49] Upon interaction with the $LiCoO_2$ nanosheet solution, the SFG spectrum of the bilayer shown in Figure 5b shows higher intensity at 2875 cm^{-1} relative to the signal of the bilayer before introduction of the nanosheets. As shown in the Supporting Information, this result is robust over five measurements and consistently shows SFG signal intensity differences of a factor of 2.0 ± 0.7. As detailed in the Supporting Information, the spectral differences were determined by calculating the area under the 2875 cm^{-1} peak.

We further investigated the effect of nanosheet concentration on the observed SFG responses. As detailed in the Supporting Information, 1 mg/L solution of $LiCoO_2$ does not significantly alter the SFG intensity at the 2875 cm^{-1} peak, while 10 mg/L solution increases the SFG signal intensity by a factor of 1.5 ± 0.6. The observed SFG responses are concentration-dependent with 5 mg/L concentration having

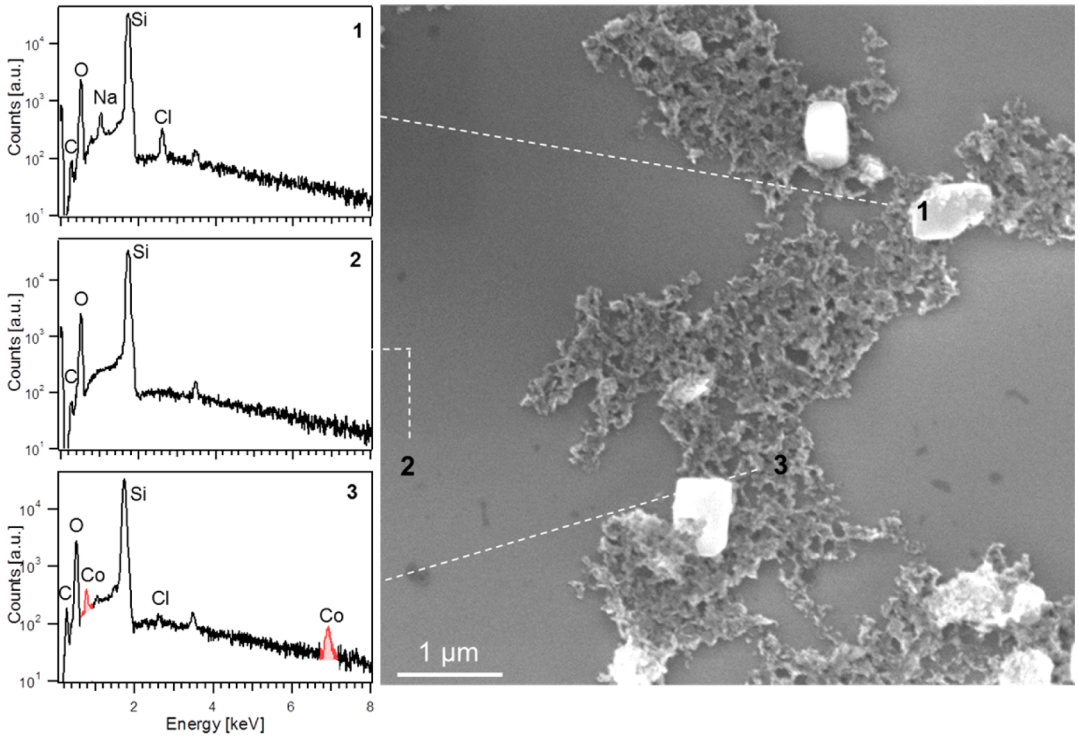

Figure 3. SEM/EDS image of a bilayer formed from 9:1 mixture of DMPC/DMPG in 0.01 M Tris buffer, 0.1 M NaCl at 23 °C and pH 7.4 upon exposure to $LiCoO_2$ nanosheets and rinsing. The large particle ("1") is NaCl, while the finer material ("3") consists of $LiCoO_2$ nanosheets.

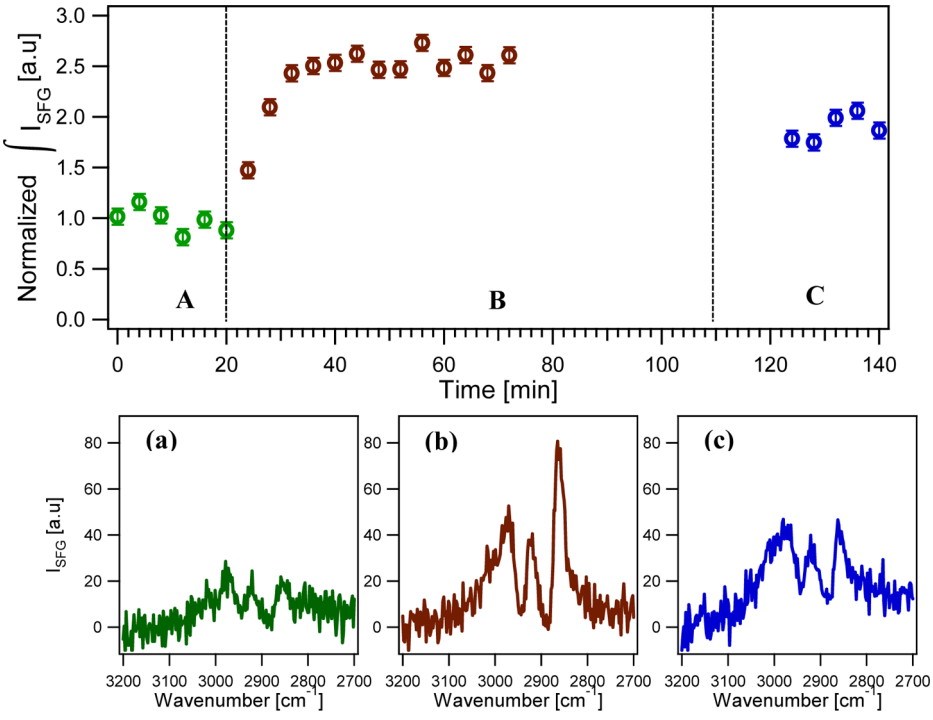

Figure 4. Normalized 2875 cm^{-1} peak area over time for bilayers formed from a 9:1 mixture of DMPC/DMPG (A) before exposure to nanosheets, (B) upon exposure to 5 mg/L of $LiCoO_2$ nanosheets, and (C) after rinsing. Representative ssp-polarized SFG spectra of bilayers formed from a 9:1 mixture of DMPC/DMPG in 0.01 M Tris buffer, 0.1 M NaCl at 23 °C and pH 7.4 (a) before exposure to nanosheets, (b) upon exposure to 5 mg/L of $LiCoO_2$ nanosheets, and (c) after rinsing. Additional spectra are shown in the Supporting Information (Figure S11).

the highest impact on the bilayer structure (see Supporting Information Figure S5).

$LiCoO_2$ nanosheets have no C−H oscillators that would contribute to the SFG signal intensity. Therefore,

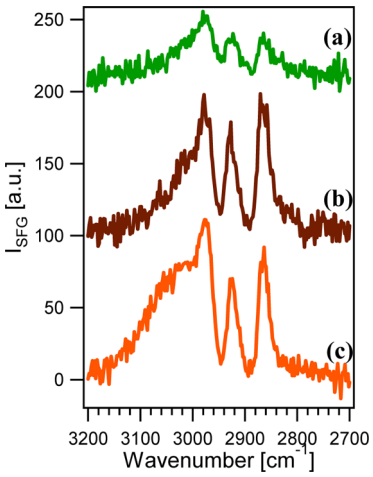

Figure 5. Representative ssp-polarized SFG spectra of bilayers formed from a 9:1 DMPC/DMPG in 0.01 M Tris buffer, 0.1 M NaCl at 23 °C and pH 7.4 (a) before the addition of nanosheets, (b) upon exposure to 5 mg/L of $LiCoO_2$ nanosheets solution, and (c) upon exposure to 5 mg/L of delithiated $LiCoO_2$ nanosheet solution. Additional spectra are shown in the Supporting Information (Figure S11).

changes in the signal intensity are due solely to the structural changes occurring at the bilayer surface upon particle attachment. The measured SFG intensity depends on the number of SFG-active C−H oscillators and their orientational average (eq 2, see Experimental Section). Provided that lipids do not leave the bilayer, probing the SFG intensity differences for a certain vibrational mode yields information about changes in bilayer symmetry. Single-component supported lipid bilayers give readily detectable SFG signals due to the fact that proximal leaflet borders the solid support and the distal leaflet borders the electrical double layer, extending into the solution. Yet, more SFG signal intensity is obtained from bilayers containing upper and lower leaflets with different densities or lipid composition, as discussed by Anglin and Conboy.[41] The results shown here suggest that leaflet asymmetry may be induced upon addition of the $LiCoO_2$ nanosheets to the bilayers formed from the 9:1 mixture of DMPC/DMPG. Additional experiments to test this hypothesis are outlined below.

DMPC/DMPS-containing Bilayers Elicit Same Response as DMPG/DMPG Containing Bilayers. As given in Supporting Information, a similar response was observed when the DMPG lipids were substituted with DMPS lipids in bilayers (Figure S6). $LiCoO_2$ nanosheets were observed to increase the SFG signal intensity from the 9:1 mixture of bilayers made of DMPC/DMPS lipids by a factor of 1.9 ± 0.5 over three measurements. In the plasma membrane, phosphatidylserine (PS) lipids are restricted predominately to the cytosolic leaflet, and the appearance of PS at the outer leaflet is associated with apoptosis.[55−57] Therefore, induced transbilayer movement of PS lipids from the inner to outer leaflet is particularly important in eukaryotic cellular membranes as it signals to macrophages to phagocytosize the cell.

TABLE 1. Diffusion Coefficients, Estimated *Z*-Average Hydrodynamic Diameters ($d_{h,Z}$),[a] and Apparent ζ-Potentials for Fresh Suspensions (5 mg/L) of Lithiated and Delithiated $LiCoO_2$ Nanosheets and NMC Nanosheets in 0.01 M Tris Buffer and 0.1 M NaCl at pH 7.4

	diffusion coefficient ($\mu m^2/s$)	$d_{h,Z}$[a] (nm)	apparent ζ-potential (mV)
$LiCoO_2$ nanosheets	0.65 ± 0.08	760 ± 79	+12.9 ± 0.6
delithiated nanosheets	0.38 ± 0.02	1320 ± 55	+0.5 ± 1.2
NMC nanosheets	0.96 ± 0.23	536 ± 155	−19.5 ± 1.4

[a] Estimate assumes spherical particles.

Delithiated $LiCoO_2$ Nanosheets Also Exhibit Strong SFG Responses from 9:1 DMPC/DMPG Bilayers. Delithiated $LiCoO_2$ nanosheets elicit similar SFG response as the $LiCoO_2$ particles (Figure 5c). Although the delithiated nanosheets exhibit a near neutral ζ-potential (+0.5 ± 1.2 mV) in contrast to the positive ζ potential of $LiCO_2$ (+12.9 ± 0.6 mV) at pH 7.4 (0.01 M Tris) in 0.1 M NaCl, adding them to the bilayers appears to elicit statistically similar increases in the SFG responses (factor of 1.7 ± 0.6 over three measurements).

Computational studies investigating the interactions between charged nanoparticles and lipid bilayers with zwitterionic headgroups suggest that nonspecific adsorption of charged nanoparticles onto phospholipid bilayers may lead to a change in the local phase (gel *vs* liquid crystalline) of the bilayer.[58−60] According to these simulations, positively charged particles are predicted to raise the effective transition temperature of the bilayer by creating a less dense upper leaflet. This situation is attributed to the van der Waals interactions between the positively charged particles (Table 1) and the zwitterionic headgroups of the lipids. Wang and co-workers offered a similar interpretation using data obtained from fluorescence microscopy,[29,61] which may, however, have been influenced by the label-specific response modifications of supported lipid bilayers that have been well-established for some spin labels by Conboy and co-workers.[41]

The phase transition temperatures for DMPC and DMPG are 24 and 23 °C, respectively. In this study, the spectra are collected at 22 ± 1 °C, where the gel and the liquid-crystalline phases coexist.[18] However, it is not clear whether the observed response is a consequence of a phase transition. The observed increases in the SFG signal intensity upon particle addition could also be due to bilayer asymmetry induced by rearrangement of the negatively charged DMPG lipids upon the addition of positively charged nanosheets. The portion of neutral or negatively charged nanosheets in the delithiated batch (recall the ζ-potential of +0.5 ± 1.2 mV, Table 1) may not interact with the bilayer, or the interaction may be dominated by

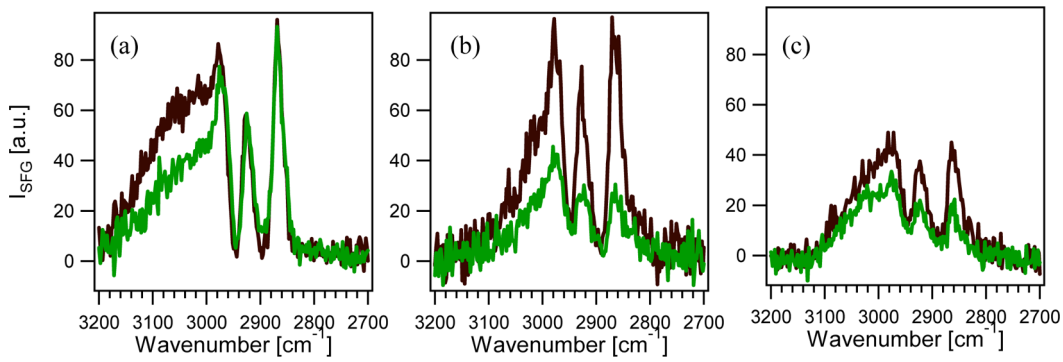

Figure 6. ssp-Polarized SFG spectra of bilayers formed from (a) 100% DMPC lipids, (b) 9:1 mixture of DMPC/DMPG lipids, (c) 8:2 mixture of DMPC/DMPG lipids, before (green) and after (brown) exposure to 5 mg/L of $LiCoO_2$ in 0.01 M Tris buffer, 0.1 M NaCl at 23 °C and pH 7.4.

entropic contributions from solvent reorganization and is the subject of future studies. The impact of the bilayer composition and the PG-specific effect on interaction will be discussed further in the following two sections.

Bilayers Made from Pure DMPC Resist Apparent Asymmetry Induction. To determine the effect of the negatively charged PG group on the SFG response from the bilayers, we investigated the interaction of lithiated and delithiated $LiCoO_2$ particles with bilayers composed of only zwitterionic DMPC lipids (no DMPG present). Before the addition of the particles, the pure DMPC bilayers exhibit vibrational features comparable to those obtained from the bilayers formed from the 9:1 mixture of DMPC/DMPG.

As shown in Figure 6a, the SFG intensity observed for the pure DMPC bilayer changes little upon exposure to $LiCoO_2$ nanosheets. This result indicates that, unlike the bilayers made from 9:1 DMPC/DMPG mixtures, the nanosheets do not induce structural change in the bilayer prepared from the purely zwitterionic PC lipids, at least as viewed by SFG spectroscopy under the conditions of our experiment, and no interaction occurs between the pure DMPC bilayer and the $LiCoO_2$ nanosheets. Although the bilayers remain intact in all cases, the observation that structural anisotropy, as measured by SFG spectroscopy, occurs only in the presence of DMPG indicates that the PG headgroup plays an important role in the interaction. Our experiment using bilayers prepared from pure DMPC (the zwitterionic lipids) effectively rules out a possible density difference between the distal and proximal leaflets as a sole mechanism for bilayer asymmetry, provided that the nanosheets are indeed present.

8:2 DMPC/DMPG Bilayers Are Also Prone to Nanosheet-Induced Asymmetrization. Our findings presented in previous sections for the bilayers prepared from the 9:1 mixture of DMPC/DMPG led us to propose a mechanism in which the concentration of the negatively charged PG lipids within each leaflet changes upon particle addition. The resultant difference in the PG concentration within the proximal *versus* the distal leaflet would then constitute enough of a compositional asymmetry that the SFG signal increases could be explained. To test this hypothesis, we increased the PG ratio in the bilayers. Figure 6c shows that once $LiCoO_2$ nanosheets are added, bilayers formed from 8:2 mixtures of DMPC/DMPG exhibit SFG signal intensity increases (a factor of 1.6 ± 0.3 over three measurements).

Anglin and Conboy previously showed that the zwitterionic PC and the phosphatidylethanolamine (PE) groups are susceptible to fast lipid flip-flop near the T_m.[41] It has also been shown that lipids having negatively charged PG headgroups are associated with an activation energy barrier lower than that of PC- and PE-terminated lipids which brings the phospholipid headgroup in the hydrophobic interior of the bilayer,[62,63] thus making negatively charged DMPG lipids more prone to flip-flop when compared to zwitterionic lipids. It is our interpretation that the electrostatic attraction between the positively charged $LiCoO_2$ particles and the negatively charged PG headgroups causes the DMPG lipids in the leaflet proximal to the fused silica support (proximal leaflet and away from particles) to flip to the distal leaflet (close to particles). This situation leaves the distal leaflet enriched in DMPG relative to the proximal leaflet, thus leading to compositional asymmetry in the bilayer and a rationale for the observed SFG signal intensity increases. A similar phenomenon of bilayer asymmetry induced by a surface-associated polypeptide was earlier demonstrated by Brown and Conboy,[49] and here we show that the effect also occurs with lithiated and delithiated cobalt oxide nanosheets. Yet, there may be a limit to leaflet enrichment with the negatively charged DMPG lipids.

The nanosheet-induced mechanism of compositional asymmetry in the bilayers also explains why the SFG signal observed at 2875 cm^{-1} does not return—on average—to the original intensity (factor of 1.4 ± 0.8 over eight measurements) after rinsing with nanosheet-free buffer solution, as shown in Figure 4c (only three out of eight runs show that the SFG signal intensity

returns back to the original bilayer intensity). This result may be attributable to the negative charges on the fused silica surface that may inhibit the negatively charged PG headgroups from returning to the proximal leaflet. Yet, the more likely reason for the disruption of lipid order to persist after rinsing is that the $LiCoO_2$ nanosheets are still present at the membrane following rinsing, as shown in the ToF-SIMS spectra in Figure 2 and the SEM image in Figure 3. The latter interpretation is relevant for biological cell membranes because they are not supported by silica substrates. Finally, we note that the SFG signal above 3000 cm^{-1}, which arises from the beginning of the O−H stretching continuum of interfacial water molecules, becomes stronger upon addition of the nanosheets. We attribute this response to differences in the interfacial water environment at the bilayer surface[64] before and after addition of the nanosheets, whose investigation is outside the scope of the present study.

NMC Nanosheets with Similar Crystal Structure Do Not Induce Apparent Asymmetry. As mentioned in the introduction, we also examined the interactions of more complex lithium intercalation compounds with the supported lipid bilayers. Specifically, we used $LiNi_{1/3}Mn_{1/3}Co_{1/3}O_2$, which is a commercially available cathode material. Unlike the previously examined metal oxide nanosheets, we found that the SFG responses from bilayers formed from our 9:1 mixture of DMPC/DMPG lipids at the H_2O (0.1 M NaCl, 0.01 M Tris buffer, pH 7.4)/silica interface are invariant with bilayer exposure to 5 mg/L of NMC nanosheets (Figure 7c, measurements made within 15 min of suspending the nanosheets). Although the NMC nanosheets are similar to the other lithium intercalation compounds in shape and crystal structure,[65] their ζ-potentials (−19.5 ± 1.4 mV) suggest that these particles carry a negative surface charge. If the NMC nanomaterial were to attach to the 9:1 DMPC/DMPG bilayers, then the negatively charged DMPG lipids would avoid Coulomb repulsion by moving from the distal (close to NMC nanomaterial) to the proximal (close to solid support) leaflet, due to the negative charge of the SiO_2 substrate. This suggests that NMC does not interact with the 9:1 DMPC/DMPG bilayers under the solution conditions used in our experiments. To obtain additional insight on the possible environmental impact of NMC nanosheet formulations, we examined the role of phosphate in the interaction. Phosphates are found in surface coatings of battery materials and are also present in aquatic environments.[16,66] Figure 7d shows that the spectral features are retained for the bilayers formed from a 9:1 mixture of DMPC/DMPG in the presence of 88.1 μM phosphate, which is common to biological growth media. NMC exposure (5 mg/L) does not alter the SFG response in the presence of phosphate either. The lack of changes in the SFG spectra upon NMC addition, with or without phosphate present, suggests that structural and compositional rearrangements within the supported lipid bilayers studied here are associated with high energy barriers that are not overcome under the conditions of the experiments, or that NMC does not interact with the bilayer in the first place. For the former case, we caution that more work is needed to quantify the amount of NMC material at the interface, which is ongoing.

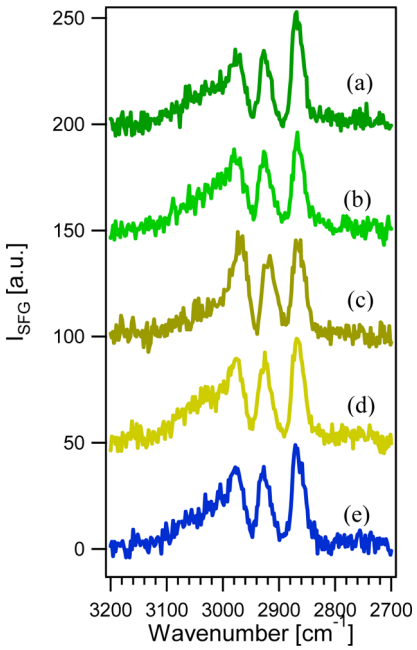

Figure 7. ssp-Polarized SFG spectra of bilayers formed from 9:1 DMPC/DMPG at 23 °C, pH 7.4 (a) in 0.01 M Tris buffer, 0.1 M NaCl, (b) in 0.01 M Tris buffer, 0.1 M NaCl, 88.1 μM Na_2HPO_4, (c) upon exposure of 5 mg/L of NMC nanosheets in 0.01 M Tris buffer, 0.1 M NaCl, (d) upon exposure of 5 mg/L of NMC nanosheets in 0.01 M Tris buffer, 0.1 M NaCl, 88.1 μM Na_2HPO_4, and (e) after rinsing with 0.01 M Tris buffer, 0.1 M NaCl, 88.1 μM Na_2HPO_4. Spectra are offset for clarity.

CONCLUSION

In summary, we have presented experimental evidence for the induction of compositional asymmetrization upon interaction of supported lipid bilayers prepared from 9:1 and 8:2 mixtures of DMPC and DMPG with lithiated and delithiated $LiCoO_2$ nanosheets while maintaining 0.1 M NaCl concentration and pH 7.4 through the use of 0.01 M Tris buffer. We find that lithiated and delithiated $LiCoO_2$ particles elicit increases in SFG signal intensity from 9:1 DMPC/DMPG bilayers, which we interpret to be due to the enrichment of negatively charged DMPG lipids in the bilayer leaflet closer to the positively charged $LiCoO_2$ nanosheets. Delithiated $LiCoO_2$ particles also exhibit strong SFG intensity increases from 9:1 DMPC/DMPG bilayers. This enrichment process may be Coulomb-limited. Bilayers made from pure DMPC, in contrast, show no apparent asymmetry induction, as reported by SFG spectroscopy, isolating the role of the negatively charged DMPG lipids in inducing the attachment

of these nanosheets and the concomitant bilayer asymmetrization, provided that the nanosheets are indeed present. Finally, we find that exposure of the bilayers to a related battery cathode material, NMC, does not result in changes to the SFG responses, independent of whether the common coanion phosphate is present.

Studying how emerging nanomaterials projected to be widely used in the near future interact with biologically relevant systems is key to understand the mechanisms of their interactions.[67] Doing so will enable the identification of possible negative consequences of introducing such materials at very large scales into the environment. Specifically, the insight that some cobalt oxide nanoformulations cause alterations to the compositional asymmetry in idealized model membranes may represent a first step toward assessing the biological consequences of their predicted widespread use. In addition, the findings presented herein contribute to molecular level insights that we argue are necessary for developing formulations enabling the sustainable use of emerging nanotechnologies.

EXPERIMENTAL SECTION

SFG Approach. The details of our SFG approach to study the nano−bio interface have been presented elsewhere.[32,68−73] Briefly, SFG is created by the temporal and spatial overlap of a tunable infrared beam and a fixed visible beam in systems that lack an inversion center, such as at interfaces. As a result, light at a frequency equal to the sum of the two incident frequencies is generated.[68,74,75] SFG provides sensitivity to molecular structures when the incident IR beam is resonant with a vibrational mode that is both Raman- and IR-active. For the purpose of our study, this condition is met in the C−H stretching frequency region (2700−3200 cm^{-1}). The intensity of the sum-frequency signal, I_{SFG}, is proportional to the square of the effective second-order nonlinear susceptibility tensor, $\chi^{(2)}_{eff}$, described by

$$I_{SFG} \propto |\chi^{(2)}_{eff}|^2 \quad (1)$$

where the susceptibility tensor depends on the orientational average of the transition dipole moments in the sample.[68,73] Due to the interfacial symmetry constraints on $\chi^{(2)}_{eff}$, SFG vibrational spectroscopy is sensitive to interfaces where inversion symmetry is inherently broken. In the study reported here, the frequency of the incident femtosecond IR light is tuned to resonance with the C−H stretches of the system, as Liu and Conboy have previously shown that the terminal CH_3 groups of the lipid alkyl chains can be used as an intrinsic probe of the symmetry of the bilayer.[37]

Here, we probe the SFG intensity due to the alkyl CH_3 symmetric stretch (ν_s) to evaluate the change in the bilayer asymmetry upon interaction with $LiCoO_2$ and delithiated $LiCoO_2$ nanosheets. The square root of the SFG intensity is proportional to SFG E-field, E_{SFG}, which, in turn, is given by the product of the effective second-order nonlinear susceptibility tensor and the applied infrared and visible electric fields, E_ω and E_ν. This product is given by the number of SFG-active C−H oscillators (N_{surf}) multiplied by their molecular hyperpolarizability tensors (β_{C-H}), averaged over all molecular orientations, according to

$$\sqrt{I_{SFG}} \propto E_{SFG} = \chi^{(2)} E_\omega E_\nu = N_{surf}\langle\beta_{C-H}\rangle \quad (2)$$

Sample Preparation. DMPC, DMPG, and DMPS were purchased from Avanti Polar Lipids and used without further purification. Lipid bilayers from small unilamellar vesicles of pure DMPC and lipid mixtures containing 9:1 DMPC/DMPG, 9:1 DMPC/DMPS, and 8:2 DMPC/DMPG (by mole) were formed on IR-grade fused silica windows (ISP Optics) *via* the vesicle fusion method, which has been previously described.[50,76] Experiments were carried out at room temperature (22 ± 1 °C). All bilayers were formed in 0.01 M Tris buffer, 0.1 M NaCl, in the presence of 0.005 M $CaCl_2$ at pH 7.40 ± 0.03, and rinsed with buffer of the same composition but lacking $CaCl_2$. The temperature and the pH were held constant throughout the experiment. Buffer solutions were filtered through a 0.2 μm PVDF membrane (Acrodisc, LC 25 mm) before each experiment. Throughout the text, we use the word "bilayer" interchangeably with "supported lipid bilayer".

$LiCoO_2$ nanosheets were synthesized by adapting a molten-salt method previously reported.[77] Varying the degree of lithiation in $LiCoO_2$ while maintaining comparable size, shape, and crystal structure is synthetically difficult. To achieve this, we used an electrochemical delithiation method, which is explained in the Supporting Information (Figure S7). Figure 1 shows the scanning electron microscopy (SEM) and transmission electron microscopy (TEM) images, indicating comparable size, shape, and crystal structure. The purified particles were further characterized by X-ray photoelectron spectroscopy and Raman spectroscopy. The characterization data are provided in the Supporting Information (Figures S8 and S9). NMC material was synthesized and characterized extensively as described elsewhere.[65]

The nanosheet suspensions ($LiCoO_2$, delithiated $LiCoO_2$, and NMC) were sonicated in a solution of 0.01 and 0.1 M NaCl at pH 7.4 for 8 min, vortexed for 30 s, and introduced into the sample cell within 15 min of suspension. Unless indicated otherwise, nanosheet solutions at 5 mg/L concentration were used in the interaction experiments due to well-formed suspensions that were stable over the time period studied, as shown in the Supporting Information Figure S10. An Ocean Optics Chem-2000 UV−vis spectrophotometer was used for absorbance measurements. UV−vis spectra shown in Figure S10 indicate only minor differences in the electronic properties of the particles maintained in the buffer solution over the time period studied. ζ-Potential measurements were obtained using Malvern Zetasizer Nano ZS. Diffusion coefficients, hydrodynamic diameters, and apparent ζ-potentials, shown in Table 1, are the averages of three measurements, each consisting of 15 runs. For ζ-potential measurements, particle suspensions (1 mL) were transferred into a clear, disposable folded capillary cell (Malvern Instruments, part no. DTS1060). Under the conditions of our experiments, lithiated and delithiated $LiCoO_2$ nanosheets possessed ζ-potentials of +12.9 ± 0.6 and +0.5 ± 1.2 mV, respectively (Table 1). We note that the $LiCoO_2$ and the delithiated $LiCoO_2$ particles suspended in ultrapure water exhibit ζ-potentials of −21.7 ± 1.2 and −19.2 ± 0.9 mV, respectively, whereas Table 1 shows the ζ-potentials for particles suspended in the buffer solution at pH 7.4. This difference is assumed to be due to the surface-active nature of the Tris cation, which has been previously recorded to be present at silica and bilayer surfaces.[50] The NMC material is associated with a ζ-potential of −19.5 ± 1.4 mV under the conditions of our experiments.

Laser, Flow Cell, and Detection System. The structural properties of the bilayers were probed by vibrational SFG using our previously published approach.[50] Briefly, substrates were placed in a Viton O-ring fitted Teflon flow cell, and the sample solutions were flowed through a reservoir across the interface with a variable flow rate controller at 2 mL/min, establishing laminar-to-creeping flow conditions within the cell.[78] The IR-grade fused silica window was cleaned in Nochromix solution (Godax Laboratories) overnight, rinsed with ultrapure water (18 Ω·cm resistivity; Millipore), and dried with N_2. The cell and the tubing were sonicated in methanol and rinsed with Millipore water. The tubing was replaced frequently to avoid

contamination. The window, O-ring, and Teflon cell were plasma cleaned (Harrick Plasma Cleaner, 18 W) for 10 min prior to use.

We used the ssp polarization combination, indicating s-polarized SFG signal, s-polarized visible light, and p-polarized IR light, to selectively probe those components of the vibrational transition dipole moments that are oriented parallel to the surface normal. SFG spectra were recorded at the supported lipid bilayer/aqueous interface with an integration time of 4 min with an average of five acquisitions. Following the pioneering approach by Esenturk and Walker,[79] we recorded each spectrum using two different center IR wavelengths to cover the relevant frequency range of interest (3200−2700 cm^{-1}). All spectra were background subtracted, calibrated to polystyrene at 2850 and 3060 cm^{-1},[79,80] and normalized to the nonresonant sum-frequency signal of a gold substrate to account for the distribution of the IR intensity.[70,81] All spectra shown in the main text and the Supporting Information were recorded at least three times.

Second Harmonic Generation Spectroscopy and Quartz Crystal Microbalance Measurements. Following the approaches described in our earlier work,[50] we also employed SHG and QCM-D measurements to monitor the interfacial electronic and mass response of the bilayers in the presence and absence of particles, respectively. There was no observed signal change upon the addition of the $LiCoO_2$ particles, as detailed in the Supporting Information (see Figures S1 and S2).

Time-of-Flight Secondary Ion Mass Spectrometry. A Phi Trift III ToF-SIMS was used for trace detection, specifically to identify lithium. The high-energy pulsed metal ions were used to bombard the sample surface, which causes the emission of secondary elemental ions from the surface. The detailed description of instrumentation can be found elsewhere.[82] A 15 keV liquid metal (Ga^+) ion gun (LMIG) with a spot size of 100 μm was used to desorb ions from the uppermost layers of a sample within an ultrahigh vacuum environment. Silica substrates were cleaned with methanol, rinsed with ultrapure water, and plasma cleaned for 5 min prior to bilayer exposure. The experiments were carried in a similar flow cell setup having 1 mL total volume and rinsed with 7 mL of buffer after the bilayer formation and particle interaction. Substrates were then left to air-dry for approximately an hour before the measurements.

Scanning Electron Microscopy. A Leo Supra55 VP scanning electron microscope was used to characterize $LiCoO_2$ particle morphology. Specifically, these images were obtained using 1 kV incident electron energy with a standard in-lens detector located above the final Gemini lens in the column of the SEM instrument. Scanning electron microscopy coupled with a Thermo Scientific UltraDry energy-dispersive X-ray spectroscopy (EDS) detector was used to characterize $LiCoO_2$ interaction with supported lipid bilayers from small unilamellar vesicles of pure DMPC and lipid mixtures containing 9:1 DMPC/DMPG formed on ultraflat SiO_2 wafers (200 nm ± 5% thermal oxide). The supported lipid bilayer exposed to $LiCoO_2$ was prepared using the same method as previously described in the sample preparation. Ultraflat SiO_2 wafers (200 nm ± 5% thermal oxide) were cleaned with ethanol, rinsed with ultrapure water, and plasma cleaned for 5 min prior to bilayer exposure. An atomic force microscopy fluid cell (Bruker MTFML-V2) was used to prepare the substrates, and the cell was rinsed with 6 mL of buffer after the bilayer formation and particle interaction. Substrates were then left to air-dry before the measurements. SEM images coupled with EDS were taken using 14 kV incident electron energy with the standard in-lens detector.

Conflict of Interest: The authors declare no competing financial interest.

Acknowledgment. This study was supported by the National Science Foundation Centers for Chemical Innovation Program, the Center For Sustainable Nanotechnology, under Grant No. CHE-1240151. The ToF-SIMS work was performed in the Keck-II facility of NUANCE Center at Northwestern University. The NUANCE Center is supported by the International Institute for Nanotechnology, MRSEC (NSF DMR-1121262), the Keck Foundation, the State of Illinois, and Northwestern University.

Supporting Information Available: The Supporting Information is available free of charge on the ACS Publications website at DOI: 10.1021/acsnano.5b01440.

General methods and additional figures (PDF)

REFERENCES AND NOTES

1. Shao-Horn, Y.; Croguennec, L.; Delmas, C.; Nelson, E. C.; O'Keefe, M. A. Atomic Resolution of Lithium Ions in $LiCoO_2$. *Nat. Mater.* **2003**, *2*, 464–467.
2. Xia, H.; Wan, Y.; Assenmacher, W.; Mader, W.; Yuan, G.; Lu, L. Facile Synthesis of Chain-Like $LiCoO_2$ Nanowire Arrays as Three-Dimensional Cathode for Microbatteries. *NPG Asia Mater.* **2014**, *6*, e126.
3. Gulbinska, M. K. *Lithium-Ion Battery Materials and Engineering: Current Topics and Problems from the Manufacturing Perspective*; Springer: London, 2014.
4. Xiao, X. L.; Yang, L. M.; Zhao, H.; Hu, Z. B.; Li, Y. D. Facile Synthesis of $LiCoO_2$ Nanowires with High Electrochemical Performance. *Nano Res.* **2012**, *5*, 27–32.
5. Wei, T.; Zeng, R.; Sun, Y. M.; Huang, Y. H.; Huang, K. V. A Reversible and Stable Flake-Like $LiCoO_2$ Cathode for Lithium Ion Batteries. *Chem. Commun.* **2014**, *50*, 1962–1964.
6. Belharouak, I.; Sun, Y. K.; Liu, J.; Amine, K. $Li(Ni_{1/3}Co_{1/3}Mn_{1/3})O_2$ as a Suitable Cathode for High Power Applications. *J. Power Sources* **2003**, *123*, 247–252.
7. Conry, T. E.; Mehta, A.; Cabana, J.; Doeff, M. M. Structural Underpinnings of the Enhanced Cycling Stability Upon Al-Substitution in $LiNi_{0.45}Mn_{0.45}Co_{0.1-Y}Al_yO_2$ Positive Electrode Materials for Li-Ion Batteries. *Chem. Mater.* **2012**, *24*, 3307–3317.
8. Goodenough, J. B.; Kim, Y. Challenges for Rechargeable Li Batteries. *Chem. Mater.* **2010**, *22*, 587–603.
9. Kang, K. S.; Meng, Y. S.; Breger, J.; Grey, C. P.; Ceder, G. Electrodes with High Power and High Capacity for Rechargeable Lithium Batteries. *Science* **2006**, *311*, 977–980.
10. Kang, D. H. P.; Chen, M.; Ogunseitan, O. A. Potential Environmental and Human Health Impacts of Rechargeable Lithium Batteries in Electronic Waste. *Environ. Sci. Technol.* **2013**, *47*, 5495–5503.
11. Poizot, P.; Laruelle, S.; Grugeon, S.; Dupont, L.; Tarascon, J. M. Nano-Sized Transition-Metaloxides as Negative-Electrode Materials for Lithium-Ion Batteries. *Nature* **2000**, *407*, 496–499.
12. Lu, Z. H.; MacNeil, D. D.; Dahn, J. R. Layered $Li\,Ni_xCo_{1-2x}Mn_xO_2$ Cathode Materials for Lithium-Ion Batteries. *Electrochem. Solid-State Lett.* **2001**, *4*, A200–A203.
13. Ruffo, R.; Wessells, C.; Huggins, R. A.; Cui, Y. Electrochemical Behavior of $LiCoO_2$ as Aqueous Lithium-Ion Battery Electrodes. *Electrochem. Commun.* **2009**, *11*, 247–249.
14. Voet, D.; Voet, J. G. *Biochemistry*, 3rd ed.; Wiley: New York, 2004.
15. Okubo, M.; Hosono, E.; Kim, J.; Enomoto, M.; Kojima, N.; Kudo, T.; Zhou, H.; Honma, I. Nanosize Effect on High-Rate Li-Ion Intercalation in $LiCoO_2$ Electrode. *J. Am. Chem. Soc.* **2007**, *129*, 7444–7452.
16. Tarascon, J. M.; Armand, M. Issues and Challenges Facing Rechargeable Lithium Batteries. *Nature* **2001**, *414*, 359–367.
17. Nel, A. E.; Madler, L.; Velegol, D.; Xia, T.; Hoek, E. M. V.; Somasundaran, P.; Klaessig, F.; Castranova, V.; Thompson, M. Understanding Biophysicochemical Interactions at the Nano-Bio Interface. *Nat. Mater.* **2009**, *8*, 543–557.
18. Liu, J.; Conboy, J. C. Asymmetric Distribution of Lipids in a Phase Segregated Phospholipid Bilayer Observed by Sum-Frequency Vibrational Spectroscopy. *J. Phys. Chem. C* **2007**, *111*, 8988–8999.
19. Stanglmaier, S.; Hertrich, S.; Fritz, K.; Moulin, J.-F.; Haese-Seiller, M.; Raedler, J. O.; Nickel, B. Asymmetric Distribution of Anionic Phospholipids in Supported Lipid Bilayers. *Langmuir* **2012**, *28*, 10818–10821.
20. Rossetti, F. F.; Textor, M.; Reviakine, I. Asymmetric Distribution of Phosphatidyl Serine in Supported Phospholipid

Bilayers on Titanium Dioxide. *Langmuir* **2006**, *22*, 3467–3473.
21. Kostarelos, K.; Lacerda, L.; Pastorin, G.; Wu, W.; Wieckowski, S.; Luangsivilay, J.; Godefroy, S.; Pantarotto, D.; Briand, J.-P.; Muller, S.; Prato, M.; Bianco, A. Cellular Uptake of Functionalized Carbon Nanotubes Is Independent of Functional Group and Cell Type. *Nat. Nanotechnol.* **2007**, *2*, 108–113.
22. Liu, W.-T. Nanoparticles and Their Biological and Environmental Applications. *J. Biosci. Bioeng.* **2006**, *102*, 1–7.
23. Marshall, A. T.; Haverkamp, R. G.; Davies, C. E.; Parsons, J. G.; Gardea-Torresdey, J. L.; van Agterveld, D. Accumulation of Gold Nanoparticles in Brassic Juncea. *Int. J. Phytorem.* **2007**, *9*, 197–206.
24. Murphy, C. J.; Gole, A. M.; Stone, J. W.; Sisco, P. N.; Alkilany, A. M.; Goldsmith, E. C.; Baxter, S. C. Gold Nanoparticles in Biology: Beyond Toxicity to Cellular Imaging. *Acc. Chem. Res.* **2008**, *41*, 1721–1730.
25. Hou, W.-C.; Moghadam, B. Y.; Corredor, C.; Westerhoff, P.; Posner, J. D. Distribution of Functionalized Gold Nanoparticles between Water and Lipid Bilayers as Model Cell Membranes. *Environ. Sci. Technol.* **2012**, *46*, 1869–1876.
26. Liu, F.; Wu, D.; Chen, K. Ligands Influence a Carbon Nanotube Penetration through a Lipid Bilayer. *J. Nanopart. Res.* **2014**, *16*, 2692.
27. Liu, Y.; Zhang, Z.; Zhang, Q. X.; Baker, G. L.; Worden, R. M. Biomembrane Disruption by Silica-Core Nanoparticles: Effect of Surface Functional Group Measured Using a Tethered Bilayer Lipid Membrane. *Biochim. Biophys. Acta, Biomembr.* **2014**, *1838*, 429–437.
28. Messersmith, R. E.; Nusz, G. J.; Reed, S. M. Using the Localized Surface Plasmon Resonance of Gold Nanoparticles to Monitor Lipid Membrane Assembly and Protein Binding. *J. Phys. Chem. C* **2013**, *117*, 26725–26733.
29. Munteanu, B.; Harb, F.; Rieu, J. P.; Berthier, Y.; Tinland, B.; Trunfio-Sfarghiu, A. M. Charged Particles Interacting with a Mixed Supported Lipid Bilayer as a Biomimetic Pulmonary Surfactant. *Eur. Phys. J. E: Soft Matter Biol. Phys.* **2014**, *37*, 14072.
30. Leroueil, P. R.; Hong, S.; Mecke, A.; Baker, J. R.; Orr, B. G.; Banaszak Holl, M. M. Nanoparticle Interaction with Biological Membranes: Does Nanotechnology Present a Janus Face?. *Acc. Chem. Res.* **2007**, *40*, 335–342.
31. Bain, C. D. Sum-Frequency Vibrational Spectroscopy of the Solid/Liquid Interface. *J. Chem. Soc., Faraday Trans.* **1995**, *91*, 1281–1296.
32. Richmond, G. L. Peer Reviewed: Vibrational Spectroscopy of Molecules at Liquid/Liquid Interfaces. *Anal. Chem.* **1997**, *69*, 536A–543A.
33. Shen, Y. R. Surface Properties Probed by Second-Harmonic and Sum-Frequency Generation. *Nature* **1989**, *337*, 519–525.
34. Liu, J.; Conboy, J. C. Structure of a Gel Phase Lipid Bilayer Prepared by the Langmuir-Blodgett/Langmuir-Schaefer Method Characterized by Sum-Frequency Vibrational Spectroscopy. *Langmuir* **2005**, *21*, 9091–9097.
35. Barth, C.; Jakubczyk, D.; Kubas, A.; Anastassacos, F.; Brenner-Weiss, G.; Fink, K.; Schepers, U.; Brase, S.; Koelsch, P. Interkingdom Signaling: Integration, Conformation, and Orientation of N-Acyl-L-Homoserine Lactones in Supported Lipid Bilayers. *Langmuir* **2012**, *28*, 8456–8462.
36. Kett, P. J. N.; Casford, M. T. L.; Davies, P. B. Sum Frequency Generation (Sfg) Vibrational Spectroscopy of Planar Phosphatidylethanolamine Hybrid Bilayer Membranes Under Water. *Langmuir* **2010**, *26*, 9710–9719.
37. Liu, J.; Conboy, J. C. Phase Transition of a Single Lipid Bilayer Measured by Sum-Frequency Vibrational Spectroscopy. *J. Am. Chem. Soc.* **2004**, *126*, 8894–8895.
38. Liu, J.; Conboy, J. C. Phase Behavior of Planar Supported Lipid Membranes Composed of Cholesterol and 1,2-Distearoyl-Sn-Glycerol-3-Phosphocholine Examined by Sum-Frequency Vibrational Spectroscopy. *Vib. Spectrosc.* **2009**, *50*, 106–115.
39. Anglin, T. C.; Brown, K.; Conboy, J. C. Creation and Relaxation of Phospholipid Compositional Asymmetry in Lipid Bilayers Examined by Sum-Frequency Vibrational Spectroscopy. *Aip. Conf. Proc.* **2010**, *1267*, 119–120.
40. Anglin, T. C.; Brown, K. L.; Conboy, J. C. Phospholipid Flip-Flop Modulated by Transmembrane Peptides Walp and Melittin. *J. Struct. Biol.* **2009**, *168*, 37–52.
41. Anglin, T. C.; Conboy, J. C. Kinetics and Thermodynamics of Flip-Flop in Binary Phospholipid Membranes Measured by Sum-Frequency Vibrational Spectroscopy. *Biochemistry* **2009**, *48*, 10220–10234.
42. Anglin, T. C.; Cooper, M. P.; Li, H.; Chandler, K.; Conboy, J. C. Free Energy and Entropy of Activation for Phospholipid Flip-Flop in Planar Supported Lipid Bilayers. *J. Phys. Chem. B* **2010**, *114*, 1903–1914.
43. Anglin, T. C.; Liu, J.; Conboy, J. C. Facile Lipid Flip-Flop in a Phospholipid Bilayer Induced by Gramicidin a Measured by Sum-Frequency Vibrational Spectroscopy. *Biophys. J.* **2007**, *92*, L1–L3.
44. Liu, J.; Brown, K. L.; Conboy, J. C. The Effect of Cholesterol on the Intrinsic Rate of Lipid Flip-Flop as Measured by Sum-Frequency Vibrational Spectroscopy. *Faraday Discuss.* **2013**, *161*, 45–61.
45. Liu, J.; Conboy, J. C. 1,2-Diacyl-Phosphatidylcholine Flip-Flop Measured Directly by Sum-Frequency Vibrational Spectroscopy. *Biophys. J.* **2005**, *89*, 2522–2532.
46. Brown, K. L.; Conboy, J. C. Lipid Flip-Flop in Binary Membranes Composed of Phosphatidylserine and Phosphatidylcholine. *J. Phys. Chem. B* **2013**, *117*, 15041–15050.
47. Chen, X. Y.; Chen, Z. SFG Studies on Interactions between Antimicrobial Peptides and Supported Lipid Bilayers. *Biochim. Biophys. Acta, Biomembr.* **2006**, *1758*, 1257–1273.
48. Yang, P.; Wu, F. G.; Chen, Z. Dependence of Alamethicin Membrane Orientation on the Solution Concentration. *J. Phys. Chem. C* **2013**, *117*, 3358–3365.
49. Brown, K. L.; Conboy, J. C. Electrostatic Induction of Lipid Asymmetry. *J. Am. Chem. Soc.* **2011**, *133*, 8794–8797.
50. Troiano, J. M.; Olenick, L. L.; Kuech, T. R.; Melby, E. S.; Hu, D.; Lohse, S. E.; Mensch, A. C.; Dogangun, M.; Vartanian, A. M.; Torelli, M. D.; Ehimiaghe, E.; Walter, S. R.; Fu, L.; Anderton, C. R.; Zhu, Z.; Wang, H.; Orr, G.; Murphy, C. J.; Hamers, R. J.; Pedersen, J. A.; Geiger, F. M. Direct Probes of 4 Nm Diameter Gold Nanoparticles Interacting with Supported Lipid Bilayers. *J. Phys. Chem. C* **2015**, *119*, 534–546.
51. Bretscher, M. S. Membrane Structure: Some General Principles. *Science* **1973**, *181*, 622–629.
52. Lygre, H.; Moe, G.; Skalevik, R.; Holmsen, H. Interaction of Triclosan with Eukaryotic Membrane Lipids. *Eur. J. Oral Sci.* **2003**, *111*, 216–222.
53. Sostarecz, A. G.; Cannon, D. M.; McQuaw, C. M.; Sun, S.; Ewing, A. G.; Winograd, N. Influence of Molecular Environment on the Analysis of Phospholipids by Time-of-Flight Secondary Ion Mass Spectrometry. *Langmuir* **2004**, *20*, 4926–4932.
54. Vaezian, B.; Anderton, C. R.; Kraft, M. L. Discriminating and Imaging Different Phosphatidylcholine Species within Phase-Separated Model Membranes by Principal Component Analysis of Tof-Secondary Ion Mass Spectrometry Images. *Anal. Chem.* **2010**, *82*, 10006–10014.
55. Devaux, P. F. Static and Dynamic Lipid Asymmetry in Cell Membranes. *Biochemistry* **1991**, *30*, 1163–1173.
56. Schlegel, R. A.; Williamson, P. Phosphatidylserine, a Death Knell. *Cell Death Differ.* **2001**, *8*, 551–563.
57. Vermes, I.; Haanen, C.; Steffensnakken, H.; Reutellingsperger, C. A Novel Assay for Apoptosis - Flow Cytometric Detection of Phosphatidylserine Expression on Early Apoptotic Cells Using Fluorescein-Labeled Annexin-V. *J. Immunol. Methods* **1995**, *184*, 39–51.
58. Prates Ramalho, J. P.; Gkeka, P.; Sarkisov, L. Structure and Phase Transformations of Dppc Lipid Bilayers in the Presence of Nanoparticles: Insights from Coarse-Grained Molecular Dynamics Simulations. *Langmuir* **2011**, *27*, 3723–3730.
59. Grillo, D.; de la Cruz, M. O.; Szleifer, I. Theoretical Studies of the Phase Behavior of Dppc Bilayers in the Presence of Macroions. *Soft Matter* **2011**, *7*, 4672–4679.
60. Van Lehn, R. C.; Alexander-Katz, A. Membrane-Embedded Nanoparticles Induce Lipid Rearrangements Similar to Those Exhibited by Biological Membrane Proteins. *J. Phys. Chem. B* **2014**, *118*, 12586–12598.

61. Wang, B.; Zhang, L. F.; Bae, S. C.; Granick, S. Nanoparticle-Induced Surface Reconstruction of Phospholipid Membranes. *Proc. Natl. Acad. Sci. U. S. A.* **2008**, *105*, 18171–18175.
62. Kol, M. A.; van Laak, A. N. C.; Rijkers, D. T. S.; Killian, J. A.; de Kroon, A. I. P. M.; de Kruijff, B. Phospholipid Flop Induced by Transmembrane Peptides in Model Membranes Is Modulated by Lipid Composition. *Biochemistry* **2003**, *42*, 231–237.
63. Homan, R.; Pownall, H. J. Transbilayer Diffusion of Phospholipids: Dependence on Headgroup Structure and Acyl Chain Length. *Biochim. Biophys. Acta, Biomembr.* **1988**, *938*, 155–166.
64. Du, Q.; Superfine, R.; Freysz, E.; Shen, Y. R. Vibrational Spectroscopy of Water at the Vapor/Water Interface. *Phys. Rev. Lett.* **1993**, *70*, 2313–2316.
65. Hang, M.; Gunsolus, I.; Wayland, H.; Melby, E. S.; Mensch, A. C.; Pedersen, J. A.; Haynes, C. L.; Hamers, R. J. Impact of Nanoscale Lithium Nickel Manganese Cobalt Oxide on the Bacterium *Shewanella oneidensis*. Manuscript in preparation
66. Nel, A. E.; Madler, L.; Velegol, D.; Xia, T.; Hoek, E. M. V.; Somasundaran, P.; Klaessig, F.; Castranova, V.; Thompson, M. Understanding Biophysicochemical Interactions at the Nano-Bio Interface. *Nat. Mater.* **2009**, *8*, 543–557.
67. Murphy, C. J.; Vartanian, A. M.; Geiger, F. M.; Hamers, R. J.; Pedersen, J.; Cui, Q.; Haynes, C. L.; Carlson, E. E.; Hernandez, R.; Klaper, R. D.; Orr, G.; Rosenzweig, Z. Biological Responses to Engineered Nanomaterials: Needs for the Next Decade. *ACS Cent. Sci.* **2015**, *1*, 117–123.
68. Lambert, A. G.; Davies, P. B.; Neivandt, D. J. Implementing the Theory of Sum Frequency Generation Vibrational Spectroscopy: A Tutorial Review. *Appl. Spectrosc. Rev.* **2005**, *40*, 103–145.
69. Geiger, F. M. Second Harmonic Generation, Sum Frequency Generation, and Chi((3)): Dissecting Environmental Interfaces with a Nonlinear Optical Swiss Army Knife. *Annu. Rev. Phys. Chem.* **2009**, *60*, 61–83.
70. Esenturk, O.; Walker, R. A. Surface Structure at Hexadecane and Halo-Hexadecane Liquid/Vapor Interfaces. *J. Phys. Chem. B* **2004**, *108*, 10631–10635.
71. Zhu, X. D.; Suhr, H. J.; Shen, Y. R. Surface Vibrational Spectroscopy by Infrared-Visible Sum-Frequency Generation. *J. Opt. Soc. Am. B* **1986**, *3*, P252.
72. Wang, H. F.; Gan, W.; Lu, R.; Rao, Y.; Wu, B. H. Quantitative Spectral and Orientational Analysis in Surface Sum Frequency Generation Vibrational Spectroscopy (SFG-VS). *Int. Rev. Phys. Chem.* **2005**, *24*, 191–256.
73. Moad, A. J.; Simpson, G. J. A Unified Treatment of Selection Rules and Symmetry Relations for Sum-Frequency and Second Harmonic Spectroscopies. *J. Phys. Chem. B* **2004**, *108*, 3548–3562.
74. Heinz, T. F. Second-Order Nonlinear Optical Effects at Surfaces and Interfaces. In *Nonlinear Surface Electromagnetic Phenomena*; Ponath, H.-E., Stegeman, G. I., Eds.; Elsevier: Amsterdam, 1991; p 353.
75. Boyd, R. W. *Nonlinear Optics*; 3rd ed.; Academic Press: London, 2008.
76. Castellana, E. T. Solid Supported Lipid Bilayers: From Biophysical Studies to Sensor Design. *Surf. Sci. Rep.* **2006**, *61*, 429.
77. Qian, D.; Hinuma, Y.; Chen, H.; Du, L.-S.; Carroll, K. J.; Ceder, G.; Grey, C. P.; Meng, Y. S. Electronic Spin Transition in Nanosize Stoichiometric Lithium Cobalt Oxide. *J. Am. Chem. Soc.* **2012**, *134*, 6096–6099.
78. Chen, E. H.; Hayes, P. L.; Nguyen, S. T.; Geiger, F. M. Zinc Interactions with Glucosamine-Functionalized Fused Silica/Water Interfaces. *J. Phys. Chem. C* **2010**, *114*, 19483–19488.
79. Esenturk, O.; Walker, R. A. Surface Vibrational Structure at Alkane Liquid/Vapor Interfaces. *J. Chem. Phys.* **2006**, *125*, 12.
80. Buchbinder, A. M.; Weitz, E.; Geiger, F. M. When the Solute Becomes the Solvent: Orientation, Ordering, and Structure of Binary Mixtures of 1-Hexanol and Cyclohexane over the (0001) Alpha-Al_2O_3 Surface. *J. Am. Chem. Soc.* **2010**, *132*, 14661–14668.
81. Buchbinder, A. M.; Weitz, E.; Geiger, F. M. Pentane, Hexane, Cyclopentane, Cyclohexane, 1-Hexene, 1-Pentene, Cis-2-Pentene, Cyclohexene, and Cyclopentene at Vapor/A-Alumina and Liquid/A-Alumina Interfaces Studied by Broadband Sum Frequency Generation. *J. Phys. Chem. C* **2010**, *114*, 554–566.
82. Willey, K. F.; Vorsa, V.; Braun, R. M.; Winograd, N. Postionization of Molecules Desorbed from Surfaces by keV Ion Bombardment with Femtosecond Laser Pulses. *Rapid Commun. Mass Spectrom.* **1998**, *12*, 1253–1260.